Propagation, blockage and coverage evaluation in 5G urban wireless networks

Anthony Salazar S.
Master in Information Technologies
Pontificia Universidad Católica del Ecuador
Quito, Ecuador
assalazars@puce.edu.ec

Germán V. Arévalo
Telecommunications Engineering
Universidad Politécnica Salesiana
Quito, Ecuador
garevalo@ups.edu.ec

René Játiva E.
Electronics Engineering Department
Universidad San Francisco de Quito
Quito, Ecuador
rjativa@usfq.edu.ec

***Abstract*—Using ray tracing and based on a set of realistic simulations performed in MATLAB ® and Open Street Maps, this document relates the coverage problem in urban 5G wireless networks with other relevant propagation and signal blockage stochastic models. From a statistical analysis of these results, the main characteristics of shadow fading are extracted and compared. In addition, a review of the current IMT-2020 and 3GPP standards on radio propagation for 5G has been carried out.**

***Index Terms*—5G wireless, propagation models, Ray Tracing, Close In, NYUSIM, coverage, standards.**

I. Introduction

The introduction of the 5G technology will transform worldwide mobile communications. 5G is a heterogeneous technology capable of cope with the increasing bit-rate demand from current and emerging network services. The increase of traffic has been particularly greater in the upstream link due to the offloading of very big amounts of data demanded from cloud-based services. Such an increase in demand overpass any previously known, including the IMT-Advanced case. In 5G, the spectral efficiency increases three times, cell peak bit-rate twenty times, and the users' bit-rate along with the density of the connections up to ten times. Besides, 5G reduces ten times latency and energy consumption. Therefore, the traffic in the 5G coverage area increments by a factor of 100 in comparison to a 4G area [1]. The enabling technologies that allow all these performance upgrades are: the use of millimetric waves (mmWave) at backhaul/fronthaul and access, the evolved-packet-core (ePC) with advanced Network Function Virtualization - Software Defined Networking (NFV/SDN) and the employ of reconfigurable wave-forms [2].

The International Telecommunications Union (ITU) [3] determines the guidelines for evaluating radio interface technologies for IMT-2020. ITU, along with the 3rd Generation Partnership Project (3GPP) [4], defines three types of scenarios for employing technologies beyond IMT-Advanced (ITU-R M.2135 [5]): For applications that overload the Mobile BroadBand (MBB) capacity, there is the enhanced Mobile BroadBand (eMBB) scenario. For deployments whose main feature is large amounts of connected devices, transmitting low volumes of delay-insensitive data, there is the Machine Type Communication (mMTC) scenario. Finally, for the deployments with strict demands of capacity, performance, latency, and availability, there is the Ultra-Reliable Low-Latency Communication (URLLC) scenario. In addition, IMT-2020 offers test environments for each one of them.

This research work focuses on a Dense Urban-eMBB test environment, simulated with Matlab® employing real-life parameters and under conditions of high density of pedestrian and vehicular users (i.e. under high traffic-loading demands). In the simulations, key parameters such as the number of antenna elements, the signal power, the bandwidth, etc., were adjusted according to the regulations reported in [3], [4]. Several channel statistical models for the characterization of both large distance and shadow fading [6], [7], [8] were considered. It was also taken into account the effects of the rain attenuation [9]. This study covers two transmission bands: 4GHz (FR1 - sub 6GHz) and 28 GHz (FR2 – mmWave) associated with their correspondent bandwidth and technical specifications. For the channel distribution, regarding the transmission or reception of data in the base station (gNB), it was employed the 3GPP TS 38.104 Rel-15 technical specification [10].

The test scenario employed in this research is a dense urban area of 4.94 squared kilometers composed of buildings, shopping centers, and corporate offices in Quito - Ecuador. The building locations and the terrain profile were retrieved from Open Street Maps (OSM) open-license software, and buildings were eventually represented by polygons, using Site Viewer from MATLAB. This procedure takes into account the terrain elevation model, the actual layout of the buildings, and the construction materials. Then, the transmitter sites are located, the antenna directivity pattern and the propagation model are defined. Finally, the transmission procedure is performed and coverage maps are obtained from the signal intensity. This methodology is valid for all models, but NYU, which does not incorporate the physical peculiarities of the terrain under study.

The main contributions of this paper are: 1) A review of the ITU and 3GPP technical specifications related to dense urban scenarios. 2) The modeling of 5G communication cells, base stations (gNB), antennas, and channel distribution, for the two representative FR1 and FR2 frequency bands [7] [11]. 3) Based on the results obtained from simulations, the paper presents the estimation, statistical validation, and comparison

of the features of a set of large distance and shadow fading models. Particularly, results from the application of Free Space [12], Close-In [13] and NYU [8] models have been contrasted with Ray Tracing simulations on a dense urban area in Quito city - Ecuador performed with the use of Open Street Maps. 4) Empirical validation of the signal blockage probability in mmWave communications from ray tracing simulations of the problem geometry to characterize the probability of the line of sight (LOS) and the probability of non line of sight (NLOS). These results are contrasted with the theoretical models, in terms of buildings density per square kilometer and statistical characterizations of the buildings dimensions. [14].

This paper is organized as follows: A brief introduction to this study and its methodology is detailed in Section I. Section II presents the most important technical specifications for each configuration and the millimeter-wave blockage analysis, in cellular networks, for both LOS and obstructed (OBS) conditions, in urban scenarios. This section also details the models for both large distance and shadow fading. Section III discusses the results obtained along this research and exhibits the curves for received signal power for the considered models. Finally, Section IV presents the most important conclusions and possible future investigations on this topic.

II. Technical specifications and simulation setup

A. ITU-R M.2412-0 specifications

IMT-2020 covers many aspects: users, manufacturers, application developers, network operators, services and content providers, and an extensive set of application scenarios. This paper focuses on the study of the Dense Urban-eMBB scenario. According to [3], the Dense Urban-eMBB test environment is composed of two layers, a macro-layer, and a micro-layer. In the macro-layer, each gNB is deployed in a regular hexagonal grid with three points of transmission and reception (TRxP), as shown in Fig. 1. In the micro-layer, for each TRxP area, there are three randomly located micro-sites. It is not defined in the ITU-R M.2412-0 specification any method for the deployment of the micro-layers. Instead, the proponent must inform the employed method and the location of the base stations of the micro-layers.

The evaluation setups for the Dense Urban-eMBB test environment are (1) evaluation of mobility and spectral efficiency and (2) evaluation of the bit rate and user experience. Scenario (1) is composed of two configurations: Setup A, for a macro-layer of 4 GHz, and Setup B, for a macro-layer of 30 GHz. Scenario (2) constitutes a setup C for one or two layers (macro + micro) for the two available frequencies: 4 GHz and 30 GHz. The carrier frequency of 4 GHz constitutes a sample of the 3 GHz to 6 GHz frequency range, and the carrier frequency of 30 GHz is a representative sample of the 24.25 GHz to 52.6 GHz range.

This paper analyzes the large distance and shadow fading for a macro-layer under Configuration A, in 4 GHz (FR1), and Configuration B, in 28 GHz (FR2). The details of these parameters are available in Table 5b in [3]. Table I exhibits the main parameters used for both configurations in our simulations.

Parameters	Config. A	Config. B
Evaluation Carrier frequency	1 layer (macro) at 4 GHz	1 layer (macro) at 30 GHz
BS antenna height (gNB)	25 m	25 m
Total transmission power for TRxP	44 dBm with a bandwidth of 20 MHz	40 dBm with a bandwidth of 80 MHz EIRP restricted to be lower than 73 dBm
Inter Site Distance (ISD)	200m	200m
UE power class	23 dBm	23 dBm, EIRP restricted to be lower than 43 dBm
Number of antenna elements per TRxP	Up to 256 Tx/ Rx	Up to 256 Tx/ Rx
Number of antenna elements of UE	Up tp 8 Tx/Rx	Up tp 32 Tx/Rx
BS Noise Figure	5 dB	7 dB
UE Noise Figure	7 dB	10 dB
Gain of BS antenna element	8 dBi	8 dBi
Gain of UE antenna element	0 dBi	5 dBi
Simulation bandwidth	20 MHz for TDD, 10 MHz + 10 MHz for FDD	80 MHz for TDD, 40 MHz + 40 MHz for FDD
UE antenna height	at outdoors: 1.5 m	at outdoors: 1.5 m

Table I
Evaluation settings for the Dense Urban-eMBB test environment

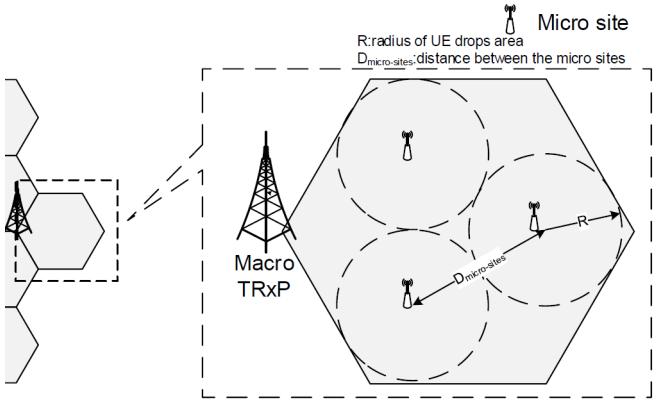

Figure 1. Reference network design for a dense urban-eMBB.

Further, for evaluation purposes, it is detailed some features of the antennas, such as the radiation pattern, the gain, the level of the pattern side lobes, and the Base Station (BS) and User Equipment (UE) antenna orientation in hexagonal and non-hexagonal grids.

The orientation of an antenna is defined as the angle, in grades, composed between the main radiation lobe and an eastern reference line. The orientation angle is measured and increased in a clockwise direction. In Table II, it is detailed the 3-TRxP BS and UE antenna radiation pattern for 30 GHz and 70 GHz. In Fig. 2 and Fig. 3 it can be seen the 3D radiation pattern, obtained in Matlab, making use of the combination method, based on the specifications presented in Table II.

Radiation Pattern for BS 3-TRxP antenna	
Parameters	**Values**
Vertical radiation pattern for antenna element (dB)	$A_{E,V}(\theta'') = \begin{bmatrix} -min[\frac{12(\theta''-90°)}{\theta_{3dB}}, SLA_V] \\ \theta_{3dB} = 65° \\ SLA_V = 30 \end{bmatrix}$
Horizontal radiation pattern for antenna element (dB)	$A_{E,H}(\phi'') = \begin{bmatrix} -min[12(\frac{\phi''}{\phi_{3dB}})^2, A_m] \\ \phi_{3dB} = 65° \\ A_m = 30 \end{bmatrix}$
Combination method for the 3D pattern of the antenna element (dB)	$\begin{bmatrix} A''(\theta'', \phi) = \\ -min(-[A_{E,V}(\theta'')] \\ +A_{E,H}(\phi''), A_m) \end{bmatrix}$
Maximum directional gain of an antenna element $G_{E,max}$	8 dBi

Table II
RADIATION PATTERN OF THE BS 3-TRXP ANTENNA

B. 3GPP TS 38.104 Rel-15 specifications

This report specifies the RF characteristics and minimum performance requirements of the New Radio (NR) BS. The bandwidth of the BS channel admits only one NR-RF carrier in the upstream and downstream link. The UE channel supports different bandwidths in the same spectral assignation, for the uplink transmissions. The bandwidth assignment of the UE channel is flexible but is limited by the BS channel-bandwidth.

Tables 5.3.2 and 5.3.3 in [10] specify the transmission-bandwidth configuration, the minimum guard bands, and numerologies for FR1 and FR2. This study also considers the following parameters, for both setups A and B as detailed

Radiation Pattern of the UE antenna at 30 GHz and 70 GHz.	
Parameters	**Values**
Radiation Pattern of the antenna element in the direction $\theta''(dB)$	$A_{E,V}(\theta'') = \begin{bmatrix} -min[\frac{12(\theta''-90°)}{\theta_{3dB}}, SLA_V] \\ \theta_{3dB} = 90° \\ SLA_V = 25 \end{bmatrix}$
Radiation Pattern of the antenna element in the direction $\phi''(dB)$	$A_{E,H}(\phi'') = \begin{bmatrix} -min[12(\frac{\phi''}{\phi_{3dB}})^2, A_m] \\ \phi_{3dB} = 90° \\ A_m = 25 \end{bmatrix}$
Combination method for the 3D pattern of the antenna element (dB)	$\begin{bmatrix} A''(\theta'', \phi) = \\ -min(-[A_{E,V}(\theta'')] \\ +A_{E,H}(\phi''), A_m) \end{bmatrix}$
Maximum directional gain of an antenna element $G_{E,max}$	5 dBi

Table III
RADIATION PATTERN OF THE UE ANTENNA AT 30 GHZ AND 70 GHZ

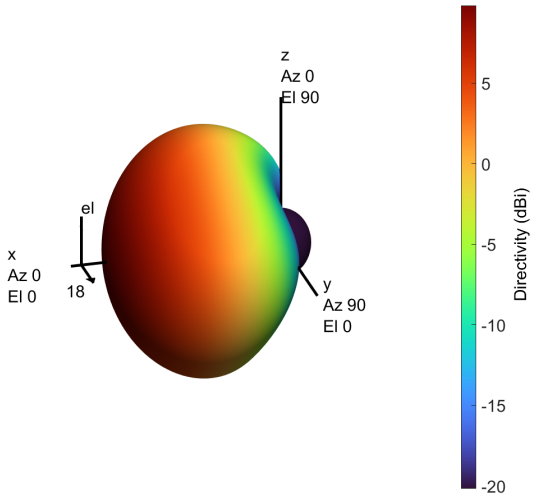

Figure 2. 3D Directivity pattern of the 3-TRxP BS antenna.

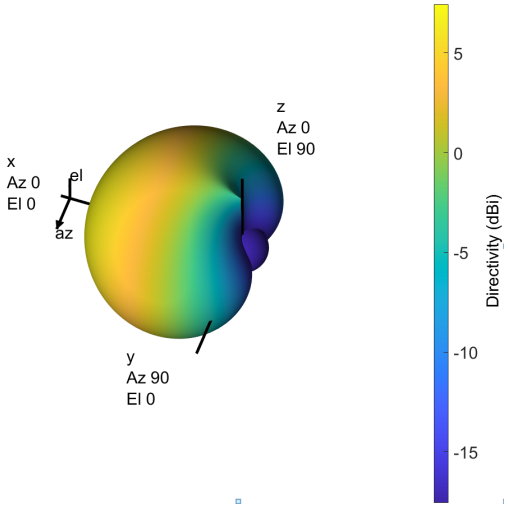

Figure 3. 3D Directivity pattern of the UE antenna, for 30 GHz and 70 GHz.

in Table III. Furthermore, Table IV and Table V detail the simulation parameters for configurations A and B respectively.

C. Analysis of signal blockage in cellular mmWave communications

The mmWave bands employed for 5G, render more difficult the communications between the transmitter and the receiver in NLOS conditions. Therefore, using stochastic geometry and

Configuration A (4 GHz)	
Parameters	**Values**
Transmission Bandwidth	20 MHz
Numerology μ	1
Sub-Carrier Spacing (SCS)	30 KHz
Ciclix Prefix (CP)	Normal
Number of Resource Blocks (N_{RB})	51
Minimum guard band	805

Table IV
SETUP A - SIMULATION PARAMETERS

Configuration B (28 GHz)	
Parameters	**Values**
Transmission Bandwidth	100 MHz
Numerology μ	3
Sub-Carrier Spacing (SCS)	120 KHz
Ciclix Prefix (CP)	Normal
Number of Resource Blocks (N_{RB})	66
Minimum guard band	2420

Table V
SETUP B - SIMULATION PARAMETERS

random shapes is possible to characterize the probability of having a LOS or instead a NLOS (obstructed) scenario in terms of the distance between transmitter and receiver. Several useful statistics for communication engineering such as the mean time a user is in NLOS may be derived from these results. Such statistics are especially useful in an urban zone where the buildings (whose positions, heights, and lengths are randomly selected) are located in parallel arrangements in such a way that they configure the shapes of the streets [14]. Some of these ideas are used in this work to empirically characterize these probabilities by using ray tracing as is commented in section III. The main feature of the shoot and bouncing rays (SBR) Ray Tracing method [15] [16] is the possibility of characterizing several reflections for the evaluation of the propagation paths. As a result, the evaluated received power using SBR at the reception sites, is more accurate modelled than statistical models. However, its computational complexity grows with the number of reflections, so they are limited to ten. SBR is generally faster than the image method.

The probability to have a LOS condition $P(LOS^x)$ is described by (1), as follows:

$$\mathbb{P}(LOS^x) = exp(\lambda \eta^x \mathbb{E}\{\mathbb{L}\} r) \tag{1}$$

where λ is the building density, $\mathbb{E}\{\}$ is the expectation operator, $\mathbb{L}$ corresponds to the random variable that describes the length of the obstacles (building fronts), r es the distance to the transmitter, and η^x is a parameter related to the blockage area and computed using stochastic geometry as in [14]. η^x depends on the distribution of the blockage heights and the transmitter and receiver antenna heights. The blockage-heights follow a uniform distribution for simulations in this paper. The probability to have an obstruction $P(NLOS^x)$ is just the complementary of $P(LOS^x)$.

D. Small-scale and large-scale propagation models

A propagation model predicts the characteristics of a radio signal, like its velocity and attenuation when propagating in some transmission media. The small-scale propagation models describe the behavior of a wave in distances comparable to its wavelength, and the large-scale propagation models describe their behavior for much longer distances.

In this research, two large-scale propagation models were employed: Free-space + hydrometeors (parameters in Table VI) and Close-in (CI); and two models with the capacity of modelling small-scale fading: SBR Ray Tracing (parameters in Table VII) and NYU-stochastic model (Table VI). However, this work focuses on propagation and signal coverage and

Rain model - gas - fog	
Parameters	**Values**
Rain rate	16 mm/h
Signal tilt angle	0 (default)
Air Temperature	23.65°
Dry air pressure	92410 Pa
Water vapor density	7.5 g/m^3
Liquid water density	0.5 g/m^3

Table VI
PARAMETERS FOR THE FREE-SPACE AND NYU PROPAGATION MODELS, IN RAIN CONDITIONS

SBR Ray Tracing Model	
Parameters	**Values**
Angular separation of the rays	media
Surface material of building geography	Concrete
Relative permittivity of building surface materials	5.31 (for concrete in a frequency range of 1-100 GHz)
Conductivity of building surface materials	0.0548 S/m
Surface material of terrain geography	Concrete
Relative permittivity of terrain materials	5.31 (for concrete in a frequency range of 1-100 GHz)
Conductivity of terrain materials	0,0548 S/m
Surface material of the Cartesian map	Plasterboard
Relative permittivity of the surface material	2.94
Conductivity of the surface material	0,0183 S/m

Table VII
PARAMETERS FOR THE SBR RAY TRACING PROPAGATION MODEL

therefore in large distance attenuation and shadow fading (random fluctuations around the mean values predicted by large distance fading models). Since Ray Tracing takes into account reflections, SBR-RT and NYU models are able to describe multipath propagation. The NYU model is also capable to model doppler shift, another small-scale effect.

Large scale propagation models predict the path loss between two remote sites, as a function of their distance. These mean path losses are described using a log model in terms of the distance and the received power at a reference LOS point located near the transmitter. Due to their stochastic formulation, these models do not consider terrain particularities neither atmospheric perturbations such as rain or fog. Particularly, CI uses a reference point located to 1 m from the transmitter, and has been adjusted to empirical data collected from almost 3000 data points from measurement campaigns performed in Aalborg University, UT Austin, NYU and Qualcomm for both LOS and NLOS environments. Therefore, CI is currently the 5G model most adjusted to reality. [17]. For simulations, setup A included the rain-model [18], and the gas-model [19] besides the free-space model. Setup B also included the fog-model [20].

For rainy conditions, it was employed some data of Quito, provided by the Meteorology and Hydrology National Institute (INAMHI).

III. RESULTS

Figure 4 presents the experimental results for blockage for an IMT-2020 antenna, placed at a height of 25 meters whose front horizon, up to 1000 meters, is an urban zone plenty of buildings and a measured building density $\lambda = 3.1592m^{-2}$. For this experiment, the Ray Tracing model with zero reflec-

tions was used and sections of area comprised between the half-power beam width (HPBW) of the antenna at the maximum distance of 600 meters were extracted with incremental ranges of 10 meters for the distance between transmitter and receiver. Within each polygon, the LOS probability was estimated as the average of the normalized powers in relation to the highest power level of the segment.The theoretical LOS probability curves were mathematically modeled as in [14].

It is evident that empiric curve achieved using ray tracing fits well with the theoretical model for dense urban scenarios, although certain minimums and maximums appear related to the particular distribution of buildings in front of the antenna. Since, the theoretical model has been validated, it may be easily used to enhance stochastic models to include building density. However, this requires a careful study that includes field measurements that ensure that the statistical model keeps on the basis of electromagnetic theory.

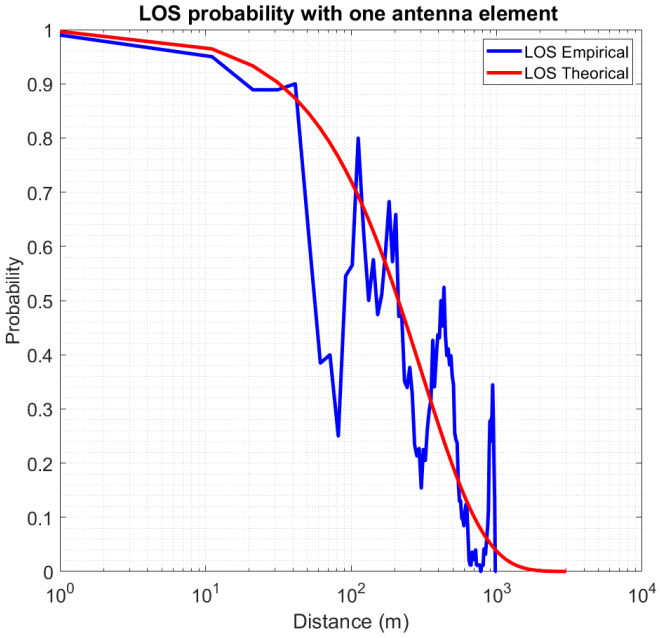

Figure 4. LOS probability with one element antenna radiation pattern.

Figure 5 shows the coverage map in the objective area using the SBR-RT technique, with 7 reflections. Lighter colors identify regions with maximum power levels, whilst zones with no color are areas with no coverage.

The received signal decay, as a function of the distance between the BS and the UE, for each propagation model employed in setups A and B. From Figure 6, it is an evident fact that the employed stochastic models accurately match the theory, with free-space loss factors close to 2, for LOS conditions, and slightly greater than 3 for NLOS conditions. Using CI and SBR-RT, the obtained loss factor is more realistic, with a value of about 2.7 for setup A at 4 MHz (Figure 6) and around 3.4 for setup B at 28 MHz (Figure 7). Besides, with SRB-RT, it is meaningfully higher the shadow

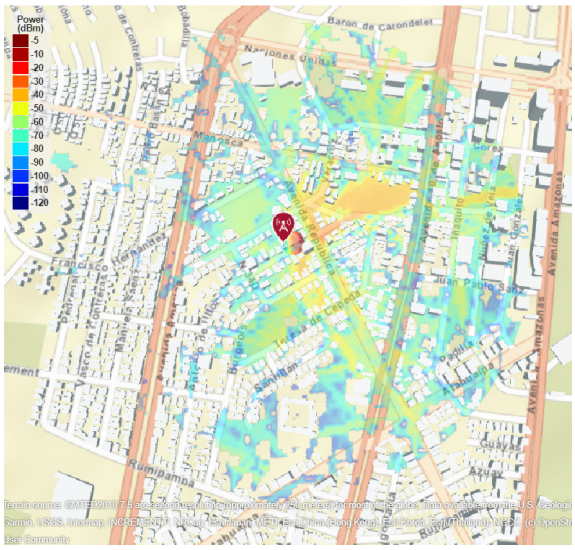

Figure 5. Coverage map with Ray Tracing SBR with 7 reflections.

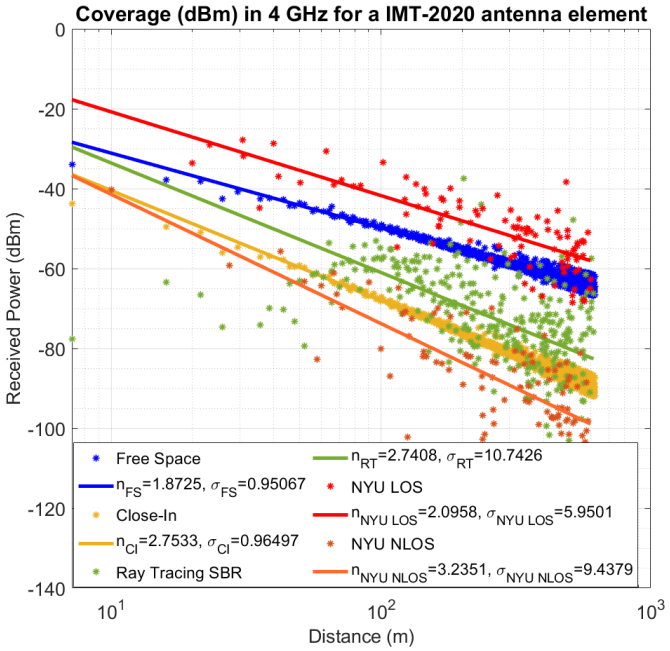

Figure 6. Coverage for different propagation models at 4 GHz.

fading dispersion. For setup B, the loss factors are higher for free-space, CI, and SBR-RT, but similar for NYU for both LOS and NLOS, with an increment of 1 dB in the shadow fading in LOS conditions. Further, the SBR-RT curves show an oscillatory behavior in the first 60 m, which may be related to the results reported in [21] for propagation models based on electromagnetic theory.

IV. Conclusions

Although it is true the fact that theoretically the path loss coefficient does not depend on the signal's frequency [21], [17], in the stochastic models adapted to realistic environments there is in fact such dependence [17]. A possible explanation

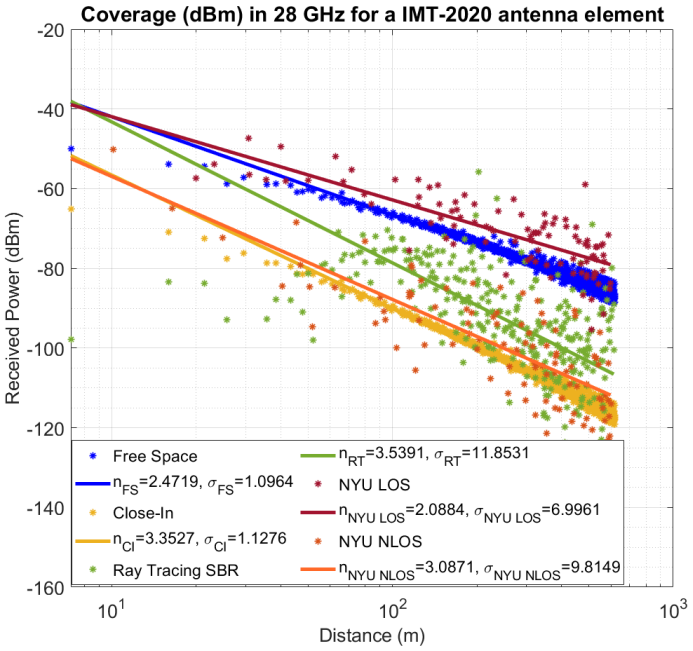

Figure 7. Coverage for different propagation models at 28 GHz.

is the coexistence of LOS and NLOS conditions, due to the geometry of the problem becomes more critical with the increase of the distance, particularly for NLOS and high frequencies. CI model seems to catch well the path loss coefficient in relation with RT simulations in this study, but penalizes signal with an additional attenuation of around 7 - 10 dB.

Acknowledgment

To Lenin Aucatoma for his support with Open Street Maps (OSM) and ICS Telecom. This work was performed with resources of UPS and USFQ Poligrant 12282.

References

[1] O. O. Erunkulu, A. M. Zungeru, C. K. Lebekwe, M. Mosalaosi, and J. M. Chuma, "5G Mobile Communication Applications: A Survey and Comparison of Use Cases," *IEEE Access*, vol. 9, pp. 97 251–97 295, 2021. [Online]. Available: https://ieeexplore.ieee.org/document/9466493/

[2] E. Calvanese Strinati, M. Mueck, A. Clemente, J. Kim, G. Noh, H. Chung, I. Kim, T. Choi, Y. Kim, H. K. Chung, G. Destino, A. Pärssinen, N. Chuberre, B. Vautherin, T. Deleu, M. Gineste, and A. Korvala, "5GCHAMPION - Disruptive 5G Technologies for Roll-Out in 2018," *ETRI Journal*, vol. 40, no. 1, pp. 10–25, Feb. 2018. [Online]. Available: http://doi.wiley.com/10.4218/etrij.2017-0237

[3] ITU, "Report ITU-R M.2412-0: Guidelines for evaluation of radio interface technologies for IMT-2020," Switzerland Patent, 2017. [Online]. Available: https://www.itu.int/dmspub/itu-r/opb/rep/R-REP-M.2412-2017-PDF-E.pdf

[4] G. O. Partners, "3GPP TR 38.913: Study on Scenarios and Requirements for Next Generation Access Technologies; (Release 16)," France Patent, 2020. [Online]. Available: https://www.3gpp.org/ftp/Specs/archive/38series/38.913/

[5] ITU, "Report ITU-R M.2135-1: Guidelines for evaluation of radio interface technologies for IMT-Advanced," Switzerland Patent, 2010. [Online]. Available: https://www.itu.int/dmspub/itu-r/opb/rep/R-REP-M.2135-1-2009-PDF-E.pdf

[6] Y. Niu, Y. Li, D. Jin, L. Su, and A. V. Vasilakos, "A Survey of Millimeter Wave (mmWave) Communications for 5G: Opportunities and Challenges," *arXiv:1502.07228 [cs]*, Feb. 2015, arXiv: 1502.07228. [Online]. Available: http://arxiv.org/abs/1502.07228

[7] A. I. Sulyman, A. T. Nassar, M. K. Samimi, G. R. Maccartney, T. S. Rappaport, and A. Alsanie, "Radio propagation path loss models for 5G cellular networks in the 28 GHZ and 38 GHZ millimeter-wave bands," *IEEE Communications Magazine*, vol. 52, no. 9, pp. 78–86, Sep. 2014. [Online]. Available: http://ieeexplore.ieee.org/document/6894456/

[8] S. Sun, T. S. Rappaport, M. Shafi, P. Tang, J. Zhang, and P. J. Smith, "Propagation Models and Performance Evaluation for 5G Millimeter-Wave Bands," *IEEE Transactions on Vehicular Technology*, vol. 67, no. 9, pp. 8422–8439, Sep. 2018. [Online]. Available: https://ieeexplore.ieee.org/document/8386686/

[9] H. Y. Lam, L. Luini, J. Din, M. J. Alhilali, S. L. Jong, and F. Cuervo, "Impact of rain attenuation on 5G millimeter wave communication systems in equatorial Malaysia investigated through disdrometer data," in *2017 11th European Conference on Antennas and Propagation (EUCAP)*. Paris, France: IEEE, Mar. 2017, pp. 1793–1797. [Online]. Available: http://ieeexplore.ieee.org/document/7928616/

[10] G. O. Partners, "3GPP TS 38.104: Base Station (BS) radio transmission and reception; (Release 15)," France Patent, 2018. [Online]. Available: https://www.3gpp.org/ftp/Specs/archive/38series/38.104/

[11] Z. Zhang, J. Ryu, S. Subramanian, and A. Sampath, "Coverage and channel characteristics of millimeter wave band using ray tracing," in *2015 IEEE International Conference on Communications (ICC)*. London: IEEE, Jun. 2015, pp. 1380–1385. [Online]. Available: http://ieeexplore.ieee.org/document/7248516/

[12] S. K. Islam and M. R. Haider, *Sensors and low power signal processing*. New York: Springer, 2010, oCLC: ocn228195902.

[13] S. Sun, T. A. Thomas, T. S. Rappaport, H. Nguyen, I. Z. Kovacs, and I. Rodrigue, "Path Loss, Shadow Fading, and Line-Of-Sight Probability Models for 5G Urban Macro-Cellular Scenarios," *arXiv:1511.07374 [cs, math]*, Nov. 2015, arXiv: 1511.07374. [Online]. Available: http://arxiv.org/abs/1511.07374

[14] C. G. Ruiz, A. Pascual-Iserte, and O. Munoz, "Analysis of Blocking in mmWave Cellular Systems: Characterization of the LOS and NLOS Intervals in Urban Scenarios," *IEEE Transactions on Vehicular Technology*, vol. 69, no. 12, pp. 16 247–16 252, Dec. 2020. [Online]. Available: https://ieeexplore.ieee.org/document/9253591/

[15] Z. Yun and M. F. Iskander, "Ray Tracing for Radio Propagation Modeling: Principles and Applications," *IEEE Access*, vol. 3, pp. 1089–1100, 2015. [Online]. Available: http://ieeexplore.ieee.org/document/7152831/

[16] K. Schaubach, N. Davis, and T. Rappaport, "A ray tracing method for predicting path loss and delay spread in microcellular environments," in *[1992 Proceedings] Vehicular Technology Society 42nd VTS Conference - Frontiers of Technology*. Denver, CO, USA: IEEE, 1992, pp. 932–935. [Online]. Available: http://ieeexplore.ieee.org/document/245274/

[17] S. Sun, T. S. Rappaport, T. A. Thomas, A. Ghosh, H. C. Nguyen, I. Z. Kovacs, I. Rodriguez, O. Koymen, and A. Partyka, "Investigation of Prediction Accuracy, Sensitivity, and Parameter Stability of Large-Scale Propagation Path Loss Models for 5G Wireless Communications," *IEEE Transactions on Vehicular Technology*, vol. 65, no. 5, pp. 2843–2860, May 2016. [Online]. Available: https://ieeexplore.ieee.org/document/7434656/

[18] ITU, "Recommendation ITU-R P.838-3: Specific attenuation model for rain for use in prediction methods," Switzerland Patent, 2005. [Online]. Available: https://www.itu.int/dmspubrec/itu-r/rec/p/R-REC-P.838-3-200503-I!!PDF-E.pdf

[19] ——, "Recommendation ITU-R P.676-11: Attenuation by atmospheric gases," Switzerland Patent, 2016. [Online]. Available: https://www.itu.int/dmspubrec/itu-r/rec/p/R-REC-P.676-11-201609-S!!PDF-E.pdf

[20] ——, "Recommendation ITU-R P.840-6: Attenuation due to clouds and fog," Patent, 2013. [Online]. Available: https://www.itu.int/dmspubrec/itu-r/rec/p/R-REC-P.840-6-201309-S!!PDF-E.pdf

[21] T. K. Sarkar, M. S. Palma, and M. N. Abdallah, *The Physics and Mathematics of Electromagnetic Wave Propagation in Cellular Wireless Communication*, 1st ed. Wiley, Jun. 2018. [Online]. Available: https://onlinelibrary.wiley.com/doi/book/10.1002/9781119393146